Separation of Soft and Hard Physics in Deeply Virtual Compton Scattering

A. Gårdestig,* A.P. Szczepaniak,† and J.T. Londergan‡

Indiana University Nuclear Theory Center, Bloomington, IN, U.S.A.

(Dated: February 1, 2008)

arXiv:hep-ph/0305210v1 19 May 2003

Abstract

A model for deeply virtual Compton scattering, based on analytical light-cone hadron wave functions is presented and studied at energies currently accessible at Jefferson Laboratory, DESY, and beyond. It is shown that perpendicular vector components play an important role at $Q^2 < 10$ GeV^2 and that the meson-exchange diagrams are important at all energies. This could significantly impact the physical interpretation of the underlying hadronic amplitudes.

PACS numbers: 13.60.Fz,13.40.-f,12.38.Bx

Keywords: Elastic and Compton scattering, Electromagnetic processes and properties, Perturbative calculations

*Electronic address:agardest@indiana.edu

†Electronic address:aszczepa@indiana.edu

‡Electronic address:tlonderg@indiana.edu

I. INTRODUCTION

Our knowledge about the partonic content of baryons has for several decades been obtained from experiments in the deep inelastic scattering (DIS) region. At sufficiently high momentum transfer, the inclusive $ep \to e'X$ reaction is very efficiently described in terms of parton distributions satisfying Bjorken scaling. The main reason for applicability of DIS to studies of hadron structure is that the process is factorizable into a hard part, calculable from perturbative quantum chromodynamics, and a soft part describing the quark-parton content of the hadron. This soft part gives the probability of finding a parton inside a proton with a certain fraction of the proton momentum. The soft part is usually parametrized in terms of parton distribution functions.

In recent years, exclusive reactions like $ep \to e'p'\gamma$ (deeply virtual Compton scattering or DVCS) or $ep \to e'p'M$ (hard electroproduction of mesons), have been explored experimentally and theoretically, since they promise to provide further insight into the parton distributions of hadrons. It turns out that even in certain exclusive reactions there is a factorization theorem that separates a hard, calculable part from a soft part [1]. It is customary to define the soft interaction by introducing generalized parton distributions (GPD's) [2, 3, 4, 5], that describe the transition amplitude for removing a parton with a certain momentum fraction and then putting it back with a different momentum fraction. The GPD's contain information about correlations between different parts of the proton wave function, or, equivalently, between partons at different locations inside the proton. This geometrical view has been explored by Burkardt, Diehl, Ralston and Pire, and others [6]. The calculations of DVCS have recently been extended to include twist-three effects [7]. The factorization of DVCS is conveniently represented by the handbag diagrams (Fig. 1), where the lower blobs are parametrized in terms of generalized parton distributions. The same diagrams have also been applied to wide angle Compton scattering and photon annihilation into hadron–anti-hadron pairs [8].

In the Bjorken limit ($Q^2 \to \infty$, $x_B = Q^2/2p\cdot q$ constant), there are four independent GPD's; $H(x,\zeta,t), E(x,\zeta,t), \widetilde{H}(x,\zeta,t)$, and $\widetilde{E}(x,\zeta,t)$, where x and ζ are respectively the light-cone momentum fractions of the struck quark and real photon, while $t = \Delta^2$ is the momentum transfer squared. Three physically different regions can be distinguished for x and ζ. The domain $0 < \zeta < x < 1$ ($\zeta - 1 < x < 0$) corresponds to the removal and return

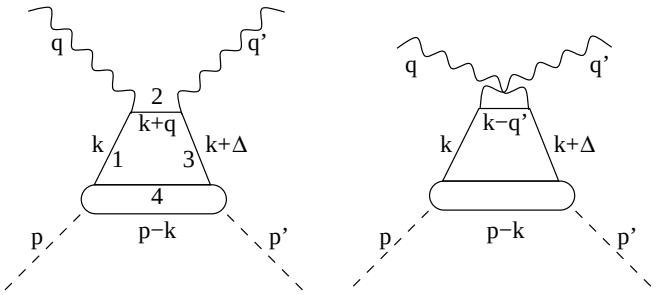

FIG. 1: The handbag diagrams, defining the kinematics and our notation.

of a quark (antiquark) with momentum fractions x ($\zeta - x$) and $x - \zeta$ ($-x$), respectively. In the remaining region $0 < x < \zeta$, the photon scatters on a virtual quark-antiquark pair, extracted from the proton. The latter situation could be described as a meson exchange, but is usually incorporated into the general parametrization of the GPD's [3, 7]. An alternative interpretation is to use light-cone perturbation theory [9] and regard the meson exchange as a higher Fock state of the proton splitting of a quark–anti-quark pair [10]. With this notation, $\zeta \to x_B$ (Bjorken x) in the limit $Q^2 \to \infty$ (Δ fixed). In the limit of forward scattering (DIS), the H's reduce to the quark density and quark helicity distributions, *e.g.* $H(x,0,0) = q(x)$ and $\widetilde{H}(x,0,0) = \Delta q(x)$. The E's do not appear in DIS. They are unique to the off-forward exclusive processes and provide information not accessible through other means. Finally the x-integrated GPD's are related to the nucleon form factors [2].

An alternative approach to DVCS using light-cone quark wave functions [9] was suggested in Refs. [10, 11]. The authors have used this idea to calculate DVCS on an electron in QED for large Q^2, assuming that the electron temporarily splits into a virtual electron-meson pair.

There are ambitious efforts under way to measure DVCS (and the hard exclusive meson photo-production) at a number of facilities, in particular at DESY [12] and JLab [13]. Experiments using high-energy muon beams are planned for the COMPASS facility at CERN [14]. At JLab energies, the competing Bremsstrahlung or Bethe-Heitler (BH) [15] process is larger than DVCS. However, by carrying out interference measurements (e^+/e^- beam charge asymmetry and various spin asymmetries), the BH amplitude cancels out and only a BH×DVCS interference remains. At DESY the energy is sufficiently large that DVCS becomes larger than BH, though the measurements have low statistics, insufficient to extract differential cross sections. However, both facilities are able to measure asymmetries for relatively low

beam energies and momentum transfers. In this paper we will investigate to what extent the 'leading' amplitude actually dominates in this kinematic region. In order to address this question, we employ a model using effective analytic quark-diquark wave functions. This model allows us to study the dynamics of the amplitudes excited at these low energies. Some preliminary results were reported in Ref. [16]. This model is similar to the one presented in Ref. [10], but we calculate DVCS on a proton and focus especially on the features at low Q^2, and we keep higher-twist terms.

II. FORMALISM

In this paper, we treat the proton as a quark-diquark state. For simplicity, we drop the proton spin degrees of freedom. Furthermore we will only consider the valence quark flavors, *i.e.*, we ignore any sea quark or higher Fock state contributions to the proton wave function. Thus, for a proton, the $SU(3)$ operator $\lambda/\sqrt{2}$ is replaced by the $SU(2)$ (isospin) operator $\tau/\sqrt{2}$. In future articles we will relax these constraints on our model, but this simplified model will suffice for the present purpose of studying the Q^2 dependence and analytic structure of the DVCS amplitudes. Our model proton state has the form

$$|p\rangle = \int \frac{dx_1 d^2\mathbf{k}_{1\perp}}{16\pi^3}\frac{dx_2 d^2\mathbf{k}_{2\perp}}{16\pi^3}\frac{16\pi^3\delta(x-x_1-x_2)\delta^2(\mathbf{k}_{1\perp}+\mathbf{k}_{2\perp})}{\sqrt{x_1x_2}} \frac{\delta_{\lambda_1\lambda_2}}{\sqrt{2}}\frac{\tau^j_{f_1f_2}}{\sqrt{2}}\frac{I_{c_1c_2}}{\sqrt{3}}\phi(x_i,\mathbf{k}_{i\perp})b^\dagger(x_1,\mathbf{k}_{1\perp})d^\dagger(x_2,\mathbf{k}_{2\perp})|0\rangle, \tag{1}$$

where λ_i, f_i, and c_i are the quark spin (helicity), flavor (isospin), and color indices. The proton state normalization is

$$\langle p'|p\rangle = 16\pi^3\delta(x'-x)\delta^2(\mathbf{p}'_\perp-\mathbf{p}_\perp). \tag{2}$$

We start from the Fourier transform of the $\gamma^* p \to \gamma p'$ amplitude (in light-cone coordinates)

$$T^{++} = -i\int d^4y e^{iq'\cdot y}\langle p'|TJ^+(y)J^+(0)|p\rangle, \tag{3}$$

where $J^+(y) = \bar\psi(y)\gamma^+\gamma_5\frac{\tau}{\sqrt{2}}\psi(y)$ is the electromagnetic current, and $p(p')$ and $q(q')$ are respectively the four-momenta of the initial (final) hadron and photon. In light-cone time-ordered perturbation theory this expression can be expanded to give the five different one-loop diagrams (assuming light-cone gauge $q^+=0$) shown in Fig. 2.

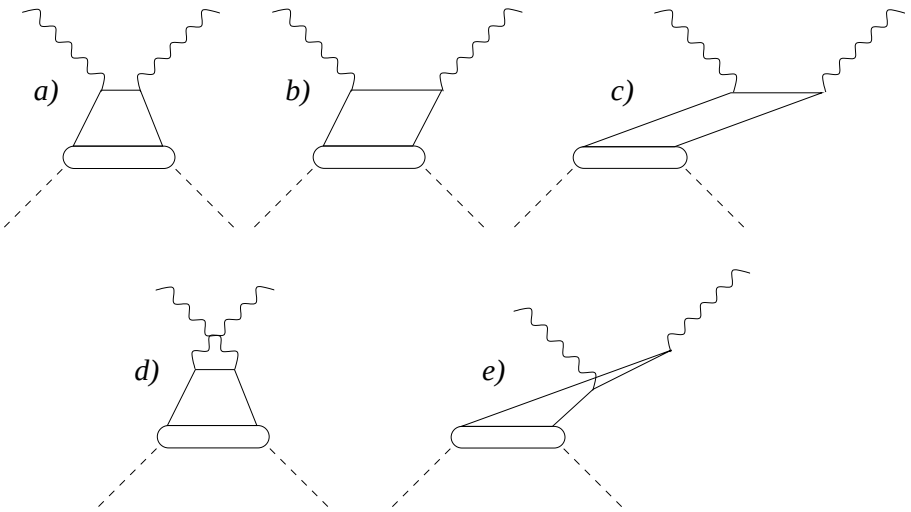

FIG. 2: The five different time-ordered 'handbag' diagrams.

These diagrams are essentially the same as those used in Brodsky *et al.* [10] for DVCS on an electron. The two approaches differ in that Brodsky *et al.* include the electron spin and treat the system as a fermion-vector composite, while we assume the diquark to be a fermion and approximate the proton as a scalar. In addition, we employ soft Gaussian form factors for our proton wave functions. The time-ordered diagrams of Fig. 2 are represented by the integrals

$$T_a^{++} = 2(p^+)^2 \int_{\zeta<x<1} \frac{dx d^2\mathbf{k}_\perp}{16\pi^3} \frac{\phi^\dagger(z,\mathbf{l}_\perp)\phi(x,\mathbf{k}_\perp)}{\left[M^2 + \left(\frac{1}{x_B}-1\right)Q^2 - \frac{m^2+\mathbf{m}_{\perp a}^{\,2}}{x} - \frac{m_R^2+\mathbf{m}_{\perp a}^{\,2}}{1-x} + i\epsilon\right]}, \tag{4}$$

$$T_b^{++} = 2(p^+)^2 \int_{0<x<\zeta} \frac{dx d^2\mathbf{k}_\perp}{16\pi^3} \frac{\left(m_R^2 - \frac{m^2+\mathbf{l}'^{\,2}_\perp}{z'} - \frac{M^2+\mathbf{l}'^{\,2}_\perp}{1-z'}\right)\varphi(z',\mathbf{l}'_\perp)\phi(x,\mathbf{k}_\perp)}{\left(-\frac{\zeta(m^2+\mathbf{m}_{\perp b}^{\,2})}{x(\zeta-x)}\right)} \times \left[M^2 + \left(\frac{1}{x_B}-1\right)Q^2 - \frac{m^2+\mathbf{m}_{\perp a}^{\,2}}{x} - \frac{m_R^2+\mathbf{m}_{\perp a}^{\,2}}{1-x} + i\epsilon\right]^{-1}, \tag{5}$$

$$T_c^{++} = 2(p^+)^2 \int_{0<x<\zeta} \frac{dx d^2\mathbf{k}_\perp}{16\pi^3} \frac{\left(m_R^2 - \frac{m^2+\mathbf{l}'^{\,2}_\perp}{z'} - \frac{M^2+\mathbf{l}'^{\,2}_\perp}{1-z'}\right)\varphi(z',\mathbf{l}'_\perp)\phi(x,\mathbf{k}_\perp)}{\left(-\frac{\zeta(m^2+\mathbf{m}_{\perp b}^{\,2})}{x(\zeta-x)}\right)\left(\frac{\Delta^2}{\zeta} - \frac{\zeta(m^2+\mathbf{m}_{\perp c}^{\,2})}{x(\zeta-x)}\right)}, \tag{6}$$

$$T_d^{++} = 2(p^+)^2 \int_{\zeta<x<1} \frac{dx d^2\mathbf{k}_\perp}{16\pi^3} \frac{\phi^\dagger(z,\mathbf{l}_\perp)\phi(x,\mathbf{k}_\perp)}{\left(\frac{1}{1-\zeta}\left(M^2 - \Delta^2 - \frac{Q^2}{x_B}\right) - \frac{(1-\zeta)\mathbf{m}_{\perp d}^{\,2}}{(x-\zeta)(1-x)} - \frac{m^2}{x-\zeta} - \frac{m_R^2}{1-x}\right)}, \tag{7}$$

$$T_e^{++} = 2(p^+)^2 \int_{0<x<\zeta} \frac{dx d^2\mathbf{k}_\perp}{16\pi^3} \frac{\left(m_R^2 - \frac{m^2+\mathbf{l}'^{\,2}_\perp}{z'} - \frac{M^2+\mathbf{l}'^{\,2}_\perp}{1-z'}\right)\varphi(z',\mathbf{l}'_\perp)\phi(x,\mathbf{k}_\perp)}{\left(-\frac{\zeta(m^2+\mathbf{m}_{\perp e}^{\,2})}{x(\zeta-x)}\right)\left(\frac{\Delta^2}{\zeta} - \frac{\zeta(m^2+\mathbf{m}_{\perp c}^{\,2})}{x(\zeta-x)}\right)}. \tag{8}$$

In Eqs. 4-8 we define the kinematic variables $z = (x-\zeta)/(1-\zeta)$, $z' = (\zeta-x)/(1-x)$, and

the relative momenta are defined as

$$\begin{aligned}
\mathbf{l}_\perp &= \mathbf{k}_\perp + (1-z)\Delta_\perp \\
\mathbf{l}'_\perp &= -(1-z')\mathbf{k}_\perp - \Delta_\perp \\
\mathbf{m}_{\perp a} &= \mathbf{k}_\perp + (1-x)\mathbf{q}_\perp \\
\mathbf{m}_{\perp b} &= \mathbf{k}_\perp + \mathbf{q}_\perp - \frac{x}{\zeta}\mathbf{q}_\perp{}' \\
\mathbf{m}_{\perp c} &= \mathbf{k}_\perp + \frac{x}{\zeta}\Delta_\perp \\
\mathbf{m}_{\perp d} &= \mathbf{k}_\perp - (1-z)\mathbf{q}_\perp{}' \\
\mathbf{m}_{\perp e} &= -\mathbf{k}_\perp - \frac{x}{\zeta}\mathbf{q}_\perp{}'.
\end{aligned} \tag{9}$$

Here $x = k^+/p^+ > 0$ and $\zeta = q'^+/p^+$ are the longitudinal momentum fractions of the struck quark and the real photon, the quantities m, m_R, and M are respectively the quark, remnant (diquark), and hadron masses, and $\Delta = q - q'$.

In the limit $Q^2 \to \infty$, the denominators of Eqs. (4) and (7) are proportional to $x - \zeta + i\epsilon$ and $x + \zeta - i\epsilon$. These are the leading twist expressions of Ji [2]. In our model these leading-twist diagrams (a and d of Fig. 2) are integrated over $\zeta < x < 1$ for which the Compton scattering occurs on a quark extracted from the proton. In principle, scattering on an anti-quark would have the same form, but it would require a different (higher Fock state) wave function. For the skew diagrams b, c, and e of Fig. 2, the photon scatters on a quark-antiquark pair split off from the proton. The proton wave function is represented by the analytic form

$$\phi(x, \mathbf{k}_\perp) = N \exp\left[-\frac{1}{\beta^2}\left(\frac{m^2}{x} + \frac{m_R^2}{1-x} + \frac{\mathbf{k}_\perp{}^2}{x(1-x)}\right)\right], \tag{10}$$

where $\beta = 0.6911$ GeV is chosen such that

$$F(q^2) = \int \frac{dx d^2\mathbf{k}_\perp}{16\pi^3}\phi(x, (1-x)\mathbf{q}_\perp + \mathbf{k}_\perp)\phi(x, \mathbf{k}_\perp) \tag{11}$$

agrees with the dipole form factor [17] for $Q^2 < 1$ GeV^2. The skew diagrams require knowledge of the wave function $\phi(z', \mathbf{l}'_\perp)$ for the diquark splitting into a hadron and quark (the lower right-hand corner of diagrams b, c, and e of Fig. 2). The form of this wave function will eventually be restricted by exclusive data, but in this paper is arbitrarily chosen to be of the form of Eq. (10), with m_R and x replaced by M and z'. Since the relative phase of the two wave functions is not known, an arbitrary complex phase factor $\exp(i\phi)$ is introduced between the regular and skew diagrams.

The full T matrix could be related to the purely kinematic T^{++} component by the Lorentz structure $T^{\mu\nu} \propto \tilde{p}^\mu \tilde{n}^\nu + \tilde{n}^\mu \tilde{p}^\nu - g^{\mu\nu}$, derived by Ji [2]. In this expression $\tilde{p}$ and $\tilde{n}$ are two lightlike four-vectors that project out the + and − components of Ji's formalism, and have been Lorentz transformed into our reference system. The Bethe-Heitler cross section is calculated from standard methods, using the dipole parametrization [17] of both the electric and magnetic proton form factors. Since we do not include the proton spin, the BH×DVCS interferences are not calculated.

III. RESULTS

The T^{++} matrix elements have been calculated for present JLab and DESY kinematics, using standard Monte Carlo techniques. These calculations incorporate both the principal value ($\Re\mathrm{e}T^{++}$) and δ-function ($\Im\mathrm{m}T^{++}$) parts. The angular distribution and Q^2 evolution of the real parts are plotted in Fig. 3. The laboratory angle $\theta_{\gamma\gamma'}$ between the virtual and real photons is defined for in-plane kinematics such that it is positive for $\phi = 0$ and negative for $\phi = 180°$, where ϕ is the azimuth angle between the final electron and the real photon, with $\hat{\mathbf{q}}$ as the polar axis. Note that this angle convention is the reverse of the one in Ref. [16].

The leading twist diagram (a of Fig. 2) is the largest for most scattering angles, with diagrams c and e giving contributions of roughly the same order. In our calculations, the contribution from the crossed diagram d is generally related to the leading-twist term by $d \sim -a/10$. This situation is quite different from DIS, where in general $d \ll a$. This difference can be understood by realizing that DVCS is an exclusive process with an on-shell off-forward final photon ($\Rightarrow \Im\mathrm{m}T_d = 0$, $\Re\mathrm{e}T_d \neq 0$), while DIS has an off-shell photon ($\Im\mathrm{m}T_d \neq 0$), so that the imaginary part of the cut diagram is the only contribution to the DIS cross section. Since we are interested in the real part of diagram d (which is absent in DIS), and DIS uses the (negligible) imaginary part (which is absent in DVCS), the two reactions turn out to be quite different and do not measure the same physics.

In the physical region of the DVCS process, diagrams a and b possess a cut on the real axis, while the other diagrams never get vanishing denominators for a massless final photon. Thus the imaginary part of the DVCS amplitude, which arises from the δ-function part of the propagators, has contributions from the first two diagrams (a and b) only. These imaginary parts are not plotted in Fig. 3 but are included in the calculation of the cross

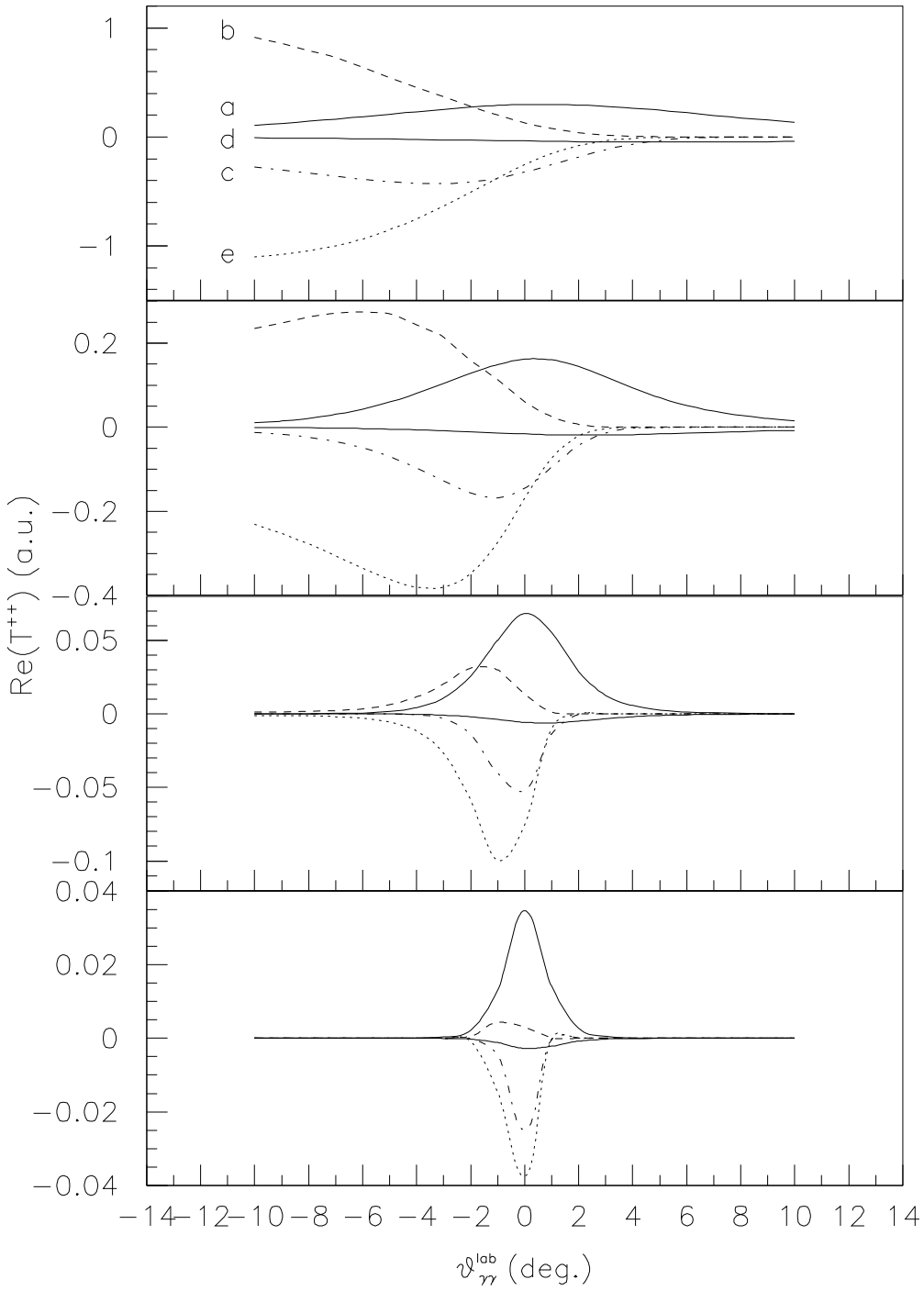

FIG. 3: The $\Re e T^{++}$ matrix elements as functions of the laboratory angle between the virtual and the real photon for in-plane scattering. The labels correspond to the ones of Fig. 2 (the lower solid line always corresponds to diagram d). The calculations are for $x_B = 0.35$ and $Q^2 = 2, 4, 10, 20$ GeV^2 from top to bottom, using an arbitrarily assigned phase angle $\phi = 0^\circ$.

section.

Because of its two hard propagators, diagram b is suppressed in the high Q^2 limit [10], and in our calculation this suppression does becomes significant, but only for large $Q^2 > 10$ GeV^2, *i.e.*, well above present JLab energies. On the other hand, diagrams c and e remain important at all energies and could be interpreted as contributing to meson exchange mechanisms, since the quark-antiquark pair could form an intermediate (off-shell) meson. The skew diagrams b, c, and e yield non-symmetric angular distributions, reflecting the shifted denominators in these cases.

The difference in analytic structure also explains why diagram d gives a smaller contribution than diagram a, since the Q^2 terms add up in the denominator of d, while they have opposite signs for a. This feature is closely related to the behavior of the two leading-twist propagators of Ji [2]. These two terms have the form $1/(x-\xi+i\epsilon)$ and $1/(x+\xi-i\epsilon)$, where x and ξ are momentum fractions related to $\frac{1}{2}(p^+ + p'^+)$ instead of p^+. In this notation there is a cancellation for $x = \xi$ (scattering on quark) or $x = -\xi$ (antiquark). The important difference between the two approaches is that Ji neglects four-vector components, *e.g.*, $\Delta_\perp$ that do not give large scalars in the Bjorken limit, while we explicitly keep them since we are interested in the behavior at low and moderate Q^2.

In Fig. 4 our predictions for the differential cross sections for DVCS and BH are shown for a range of beam energies, and for various choices of the relative phase between the regular and skew diagrams. These plots are comparable to those published in [3] for the kinematics corresponding to the JLab [13], DESY [12], and CERN [14] experiments. Only for very large Q^2 is it possible to separate DVCS from BH when only unpolarized cross sections are available. The dip in the DVCS cross section at $\approx 2^\circ$ for zero phase angle reflects the fact that the real parts add up to zero there. If such a structure would be observed (at large beam energies), it could help constrain the phase between the regular and skew diagrams.

The effect of the skew diagrams on the cross section is seen Fig. 5. When they are removed (lower graph, solid line), the dip in the cross section disappears, but the cross section for backward angles also decreases by roughly an order of magnitude. However, the cross section is still asymmetric. If in the remaining leading twist diagrams a and d we set $\mathbf{k}_\perp = 0$ in the energy denominators (lower graph, dashed line), we end up with a narrower, almost symmetric distribution. At small angles this shift increases the cross section by 30–40% and for backward angles it decreases it by a factor of about two.

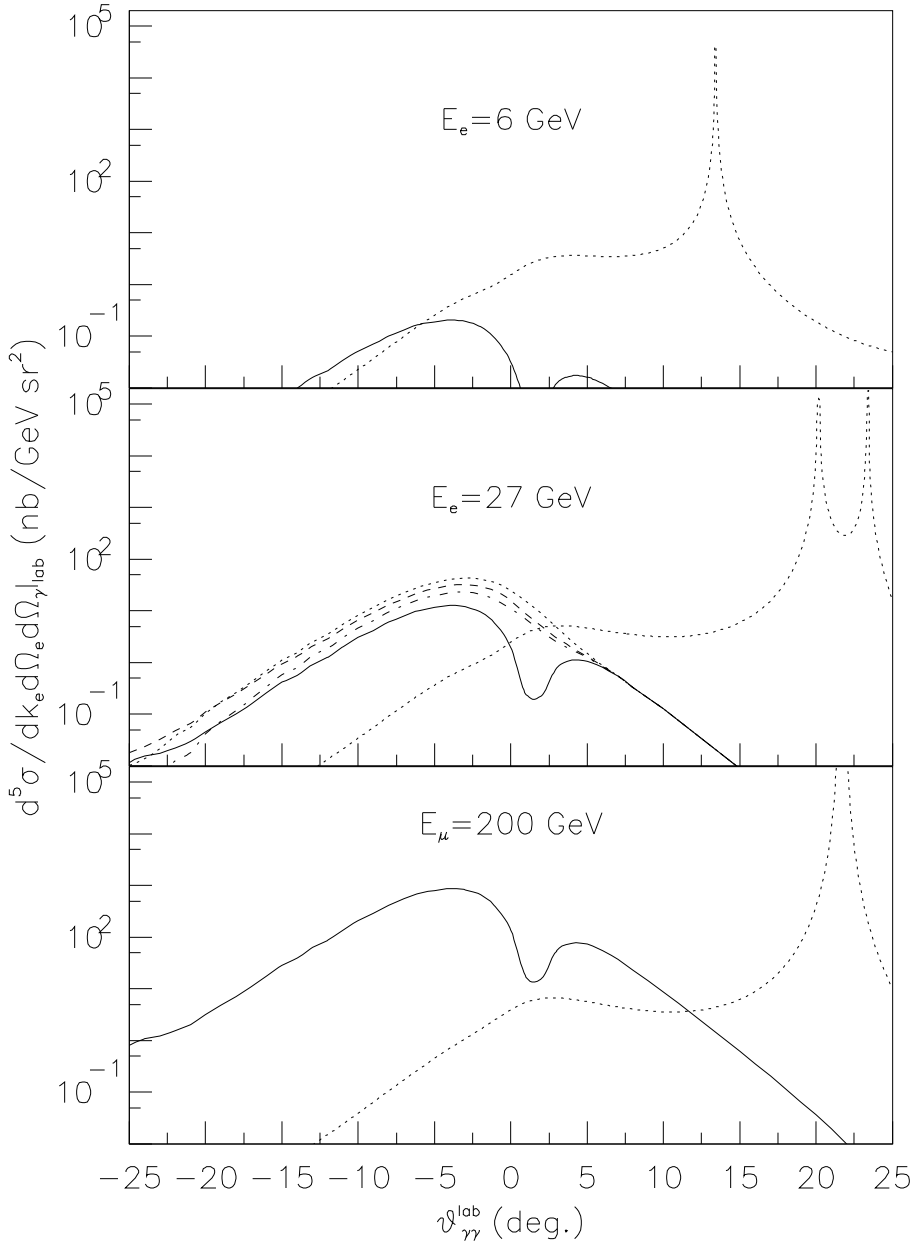

FIG. 4: Differential cross section for DVCS (solid line) and BH (right-most dotted line) at $x_B = 0.3$, $Q^2 = 2$ GeV^2, and beam energies of the JLab, DESY, and CERN experiments. In the second graph the phase between diagrams a, d and b, c, e is 0° (solid line), 90° (dashed line), 180° (dotted line), and 270° (dot-dashed line).

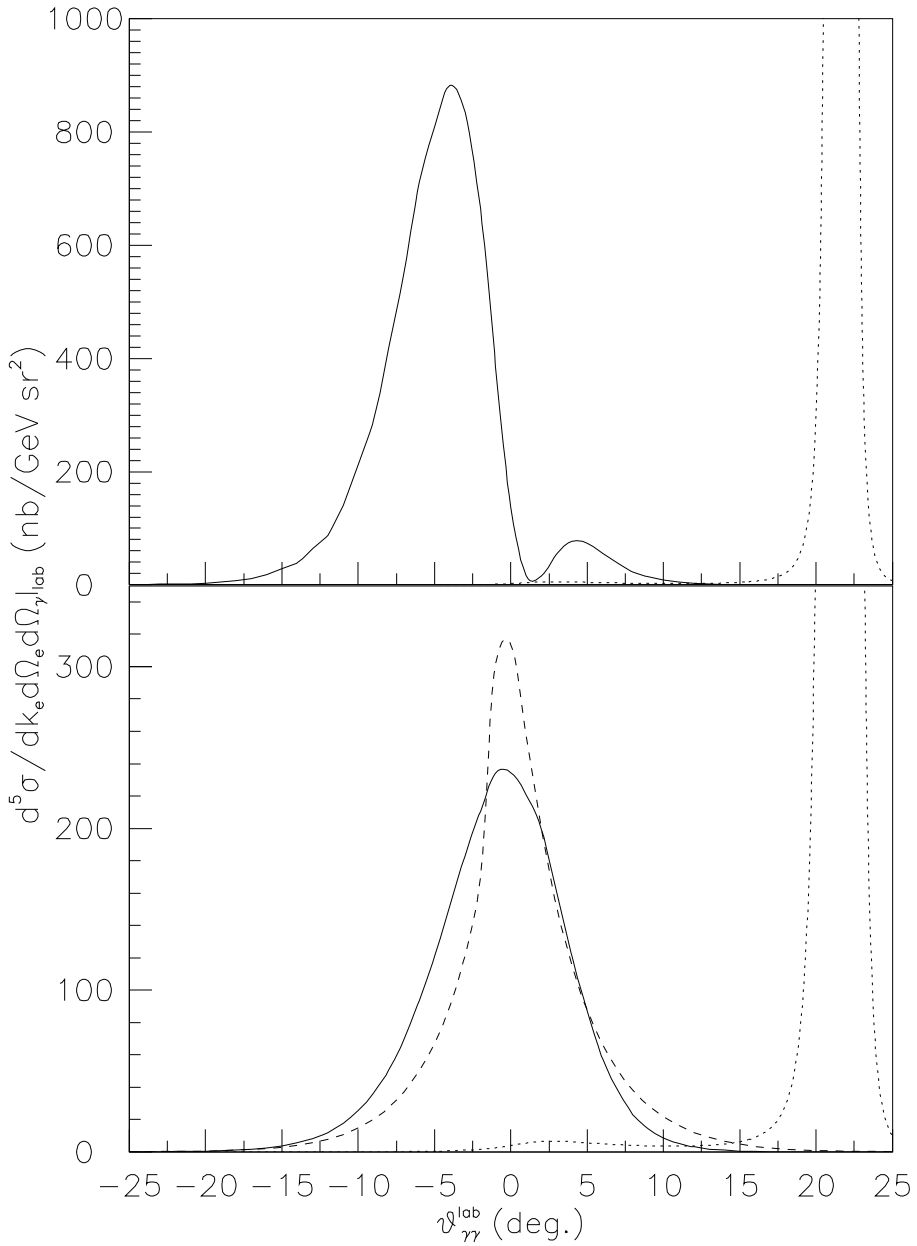

FIG. 5: Effect of excluding the skew diagrams, for energy $E_\mu = 200$ GeV. Upper graph: skew diagrams included. Lower graph, only the leading twist diagrams a and d are included. Lower graph, dashed line: only leading twist diagrams, and setting $\mathbf{k}_\perp = 0$ in the denominators (dashed line). Note that the two plots use different linear scales.

The skewed behavior of the angular distribution is hence caused by a combination of two effects; the backward shifted meson exchange (skew) diagrams, and the presence of perpendicular components in the propagators.

IV. CONCLUSIONS AND OUTLOOK

We have introduced a model for DVCS, using simple analytic quark wave functions and retaining all components of every four-vector in the scattering process. This model enables us to investigate the five single-loop diagrams and their relative importance for DVCS at JLab and HERA energies. Our results indicate that at present JLab energies ($Q^2 < 4$ GeV^2), all of the diagrams of Fig. 2 (except possibly the crossed diagram d) contribute to the DVCS cross sections. In particular it is necessary to include diagram b, despite its two hard propagators, since the suppression of this amplitude is significant only for very large Q^2. Even at kinematics appropriate for the upgraded (12 GeV) JLab, the maximal $Q^2 \sim 6$ GeV^2 is too small to suppress diagram b. Other higher-order diagrams might need to be considered as well. At higher values $Q^2 > 10$ GeV^2, the process is completely dominated by the handbag diagrams with one hard propagator. The crossed, u-channel diagram d of Fig. 2 contributes on the 10% level. This should be contrasted with DIS, where this amplitude is very small and negligible. In our calculations the skew diagrams c and e are of the same order as the regular handbag a for all Q^2. Consequently, meson exchange mechanisms are likely to be important for the understanding of DVCS.

In the case of DIS, where cross sections are given by the imaginary part of the forward $\gamma^* N \to \gamma^* N$ amplitude, in the scaling region the t-channel meson exchange is relevant only at small x_B. In the limit of large s and low t, where $s = Q^2(1 - x_B)/x_B$, the amplitude is expected to be dominated by the right-most singularity in the complex-l plane. This leads to an amplitude proportional to $\beta_n(Q^2)(Q/x_B m_N)^{\alpha_n(0)}$. Due to the large photon virtuality, however, the Regge residues $\beta_n(Q^2)$ are suppressed for high spin states $\beta_n(Q^2) \sim (1/Q)^{\alpha_n(0)}$. This simply follows from the t-channel sub-process amplitudes, $\gamma^*(q)\gamma^*(q') \to n_l$, where $l = \alpha(m_n^2)$

$$\beta_n(Q) \sim A(\gamma^*\gamma^* \to n_l) \propto \int d^3\mathbf{k} P_l(\hat{\mathbf{k}} \cdot \hat{\mathbf{q}}) \frac{\phi_n(\mathbf{k})}{(k - (q + q')/2)^2} \propto \left(\frac{1}{Q}\right)^l . \tag{12}$$

Thus, for DIS processes the Regge limit only applies at low x_B, while at finite x_B an

alternative (parton) description becomes more efficient. In the case of DVCS, however, the presence of the real photon in the exit channel invalidates the above argument, since the residue functions, $\beta_n(Q) \sim A(\gamma^*\gamma \to n_l) \propto 1/Q^2$ are not suppressed for high spin states [18]. In other words, the presence of the soft $q \to Nq$ fragmentation described by the bottom-right part of diagrams c and e masks the simple interpretation of the DVCS process in terms of partons originating from the nucleon alone.

We have shown that the perpendicular components of four vectors significantly alters the angular distribution of DVCS, and makes it skew toward backward angles. This effect is further enhanced by the inclusion of the skew diagrams.

This work will be extended to include a full treatment of the proton spin. This will allow us to calculate the interference of DVCS with the Bethe-Heitler process and hence to calculate spin asymmetries, which are needed for a thorough comparison with data. With this extended model, we will again test the validity of commonly applied approximations, and we will evaluate the effectiveness of various proton wave functions. We also intend to calculate meson photoproduction, with special consideration of the meson poles that appear in the skew diagrams.

In conclusion, our calculations show that higher twist effects should be important in DVCS processes particularly at the relatively low energies currently accessible at JLab. In this kinematic region, higher twist amplitudes need to be carefully studied and calculated. In addition, a substantial part of the intuition we bring from DIS processes may no longer be valid in evaluating DVCS processes.

Acknowledgments

One of the authors (A.P.S.) would like to thank M. Burkardt for valuable discussions. This work was supported in part by NSF grant nsf-phy0070368 and DOE grant DE-FG02-87ER40365.

---

[1] J.C. Collins and A. Freund, Phys. Rev. D **59**, 074009 (1999); X. Ji and J. Osborne, Phys. Rev. D **58**, 094018 (1998); A.V. Radyushkin, Phys. Rev. D **56**, 5524 (1997).

[2] X. Ji, Phys. Rev. Lett. **78**, 610 (1997); Phys. Rev. **D55**, 7114 (1997).

[3] P.A.M. Guichon and M. Vanderhaeghen, Prog. Part. Nucl. Phys. **41**, 125 (1998); M. Vanderhaeghen, P.A.M. Guichon, and M. Guidal, Phys. Rev. D **60**, 094017 (1999); K. Goeke, M.V. Polyakov, and M. VanderHaeghen, Prog. Part. Nucl. Phys. **47**, 401 (2001).

[4] A.V. Radyushkin, Phys. Rev. D **58**, 114008 (1998).

[5] M. Diehl, T Feldmann, R. Jakob, and P. Kroll, Eur. Phys. J. **C8**, 409 (1999).

[6] M. Burkardt, Nucl. Phys. **A711**, 127 (2002); M. Diehl, Eur. Phys. J. **C25**, 223 (2002); J.P. Ralston and B. Pire, Phys. Rev. D **66**, 111501 (2002).

[7] A.V. Belitsky, D. Müller, and A Kirchner, Nucl. Phys. **B629**, 323 (2002).

[8] H.W. Huang, P. Kroll, and T. Morii, Eur. Phys. J. **C23**, 301 (2002); M. Diehl, P. Kroll, and C. Vogt, Eur. Phys. J. **C26**, 567 (2003); M. Diehl, P. Kroll, and C. Vogt, Phys. Lett. **B532**, 99 (2002).

[9] G.P. Lepage and S.J. Brodsky, Phys. Rev. D **22**, 2157 (1980); S.J. Brodsky, H. Pauli, and S.S. Pinsky, Phys. Rept. **301**, 299 (1998).

[10] S.J. Brodsky, M. Diehl, and D.S. Hwang, Nucl. Phys. **B596**, 99 (2001).

[11] M. Diehl, T Feldmann, R. Jakob, and P. Kroll, Nucl. Phys. **B596**, 33 (2001).

[12] A. Airapetian *et al.*, Phys. Rev. Lett. **87**, 182001 (2001).

[13] S. Stepanyan *et al.*, Phys. Rev. Lett. **87**, 182002 (2001).

[14] M. d'Hose *et al.*, Acta Phys. Pol. **B33**, 3773 (2002).

[15] L.W. Mo and Y.S. Tsai, Rev. Mod. Phys. **41**, 205 (1969).

[16] A. Gårdestig, A.P. Szczepaniak, and J.T. Londergan, in *Exclusive Processes at High Momentum Transfer*, Workshop Proceedings, Eds. A. Radyushkin and P. Stoler, (World Scientific, Singapore, 2002), p. 124; `hep-ph/0209232`.

[17] O. Dumbrajs *et al.*, Nucl. Phys. **B216**, 277 (1983).

[18] V.L. Chernyak, A.R. Zhitnitsky, Phys. Rept. **112**, 173 (1984).